One-neutron knockout reactions on proton-rich nuclei with $N=16$

A. Gade,[1,2] D. Bazin,[1] B. A. Brown,[1,2] C. M Campbell,[1,2] J. A. Church,[1,2] D. C. Dinca,[1,2] J. Enders,[1,*] T. Glasmacher,[1,2] P. G. Hansen,[1,2] Z. Hu,[1,†] K. W. Kemper,[3] W. F. Mueller,[1] H. Olliver,[1,2] B. C. Perry,[1,2,‡] L. A. Riley,[4] B. T. Roeder,[3] B. M. Sherrill,[1,2] J. R. Terry,[1,2] J. A. Tostevin,[5] and K. L. Yurkewicz[1,2]

[1]*National Superconducting Cyclotron Laboratory, Michigan State University, East Lansing, Michigan 48824, USA*

[2]*Department of Physics and Astronomy, Michigan State University, East Lansing, Michigan 48824, USA*

[3]*Department of Physics, Florida State University, Tallahassee, Florida 32306, USA*

[4]*Department of Physics and Astronomy, Ursinus College, Collegeville, Pennsylvania 19426, USA*

[5]*Department of Physics, School of Electronics and Physical Sciences, Guildford, Surrey GU2 7XH, United Kingdom*

(Received 18 September 2003; published 8 March 2004)

One-neutron knockout reactions from the deeply bound $N=16$ isotones with $Z=16,17$, and 18 have been studied in inverse kinematics with intermediate-energy beams. γ-ray spectroscopy in coincidence with the detection of knockout residues allowed for an investigation of the one-neutron removal leading to individual excited states. Spectroscopic factors are deduced in the framework of the sudden and eikonal approximations and are compared to USD shell-model predictions. The momentum distributions observed in the experiment are used to identify the angular momentum l carried by the knockedout neutron by comparing with calculations based on a black-disk reaction model. The systematics of reduced single-particle occupancies attributed to the effect of short-range correlations, observed so far for stable and near-magic nuclei in $(e,e'p)$ and $(d,{}^3\mathrm{He})$ reactions and in one-nucleon knockout on light deeply bound systems, are extended in this work.

DOI: 10.1103/PhysRevC.69.034311 PACS number(s): 24.50.+g, 21.10.Jx, 27.30.+t

I. INTRODUCTION

Single-nucleon knockout reactions in inverse kinematics have already proven their outstanding capability to provide detailed experimental information on the single-particle structure of rare nuclear species away from the valley of β stability [1–3]. In addition to the study of the structure of halo nuclei [4,5] and the search for the breakdown of shell closures for nuclei in the regime of extreme N/Z [6], spectroscopic factors for individual single-particle states have been deduced using this experimental approach [7–10].

At intermediate beam energies ($\geqslant$50 MeV/nucleon), a theoretical description in the framework of straight-line trajectories (eikonal approach) and sudden approximation is possible. Therefore, the model dependency is reduced compared to the classical low-energy transfer reactions, as for example (p,d) and $(d,{}^3\mathrm{He})$, whose calculation involves the distorted-wave Born approximation or higher-order formalisms, and which depend strongly on the entrance and exit channel optical model potentials [11].

For stable nuclei the $(e,e'p)$ reaction has been established as providing precision information on spectroscopic factors of proton single-particle states. It has been observed that the spectroscopic factors determined experimentally are systematically smaller by a factor of 0.50–0.60 with respect to the prediction of the independent-particle shell model [12]. This is attributed to the incomplete treatment of the short-range correlations resulting from the strongly repulsive core and the tensor part of the nucleon-nucleon interaction within the conventional shell model using effective interactions [13]. It has been shown recently that transfer reactions such as $(d,{}^3\mathrm{He})$ can be reanalyzed in a consistent way and yield the same reduction in the deduced single-particle strength [14].

A completely different situation holds in the regime of low binding energies. The observed reduction is closer to 0.9 and suggests that the effect of the short-range correlations is less apparent for weakly bound states [2,3,15].

In this paper we report the study of proton-rich nuclei with $Z=16,17$, and 18 using the one-neutron knockout reactions $^9\mathrm{Be}(^{32}\mathrm{S},{}^{31}\mathrm{S}+\gamma)\mathrm{X}$, $^9\mathrm{Be}(^{33}\mathrm{Cl},{}^{32}\mathrm{Cl}+\gamma)\mathrm{X}$, and $^9\mathrm{Be}(^{34}\mathrm{Ar},{}^{33}\mathrm{Ar}+\gamma)\mathrm{X}$ in inverse kinematics. These cases have higher neutron-separation energies, 15.04, 15.74, and 17.07 MeV, respectively, than those studied before. This makes the cross sections smaller and the momentum distributions for different l less distinct but still distinguishable. A detailed discussion of residue momentum distributions, inclusive cross sections, cross sections to individual final states, and the reduction of the experimentally observed spectroscopic strength with respect to USD shell-model predictions will be presented for these deeply bound systems with neutron-separation energies exceeding 15 MeV.

II. EXPERIMENT

An exotic multicomponent beam consisting of the $N=16$ isotones $^{32}\mathrm{S}$, $^{33}\mathrm{Cl}$, and $^{34}\mathrm{Ar}$ was obtained by fragmentation of a 150 MeV/nucleon $^{36}\mathrm{Ar}$ primary beam provided by the Coupled Cyclotron Facility at the National Superconducting Cyclotron Laboratory (NSCL). The fragmentation target (1034 mg/cm^2 $^9\mathrm{Be}$) was located at the midacceptance target

*Present address: Institut für Kernphysik, TU Darmstadt, D-64289 Darmstadt Germany.

†Present address: School of Medicine, University of Utah, Salt Lake City, UT 84112.

‡Present address: Constellation Technologies, Largo, FL 33777.

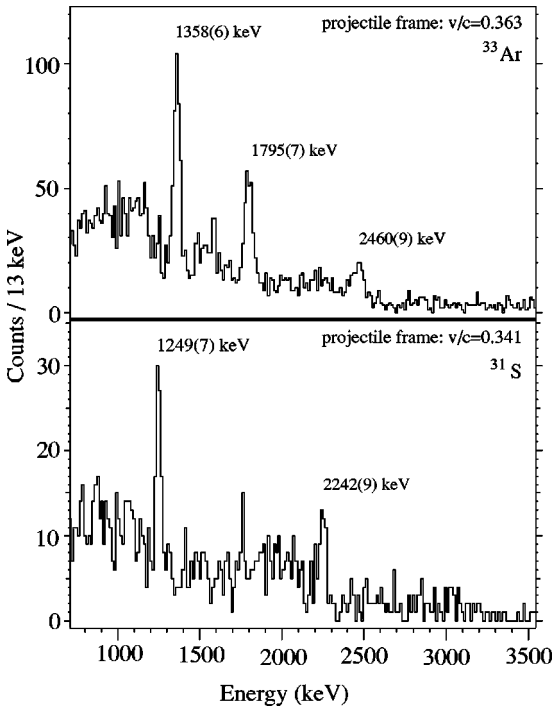

FIG. 1. γ spectra event-by-event Doppler reconstructed into the projectile frame detected in coincidence with the residues ^{33}Ar (upper panel) and ^{31}S (lower panel). The γ rays observed depopulate known excited states in these $N=15$ isotones. The excess of counts around 1740 keV in the ^{31}S spectrum does not correspond to a known transition in ^{31}S and might be attributed to one of the higher-lying fragmented $5/2^+$ states expected to be populated in one-neutron knockout according to shell-model calculations (see text for details).

position of the large-acceptance A1900 fragment separator [16].

The secondary 188(4)mg/cm^2 ^{9}Be target was placed at the target position of the S800 spectrograph [17] and surrounded by SeGA (Segmented Germanium Array), presently the largest operational highly segmented Germanium detector array for in-beam γ-ray spectroscopy with fast exotic beams. Fifteen 32-fold segmented HPGe detectors [18] were arranged at a distance of 20 cm from the secondary target in two rings with central angles of 90° and 37° relative to the beam axis. The high degree of segmentation together with the geometry of the setup resulted in a segment opening angle of about 2.7°, thus allowing for an accurate event-by-event Doppler reconstruction of the γ rays emitted in flight. The γ-ray spectra detected in coincidence with the knockout residues and event-by-event Doppler reconstructed into the projectile frame are displayed in Figs. 1 and 2.

The configuration with eight detectors in the 90° ring and seven in the 37° ring provided a total photopeak efficiency of 2.0% at 1.33 MeV γ-ray energy. GEANT3 [19] simulations successfully modeled the efficiency of the array determined with standard calibration sources at rest and provided the detector response for in-beam data by taking into account the Lorentz boost arising from the velocity of the reaction residues at the moment of the γ-ray emission (v/c between 0.341 and 0.363).

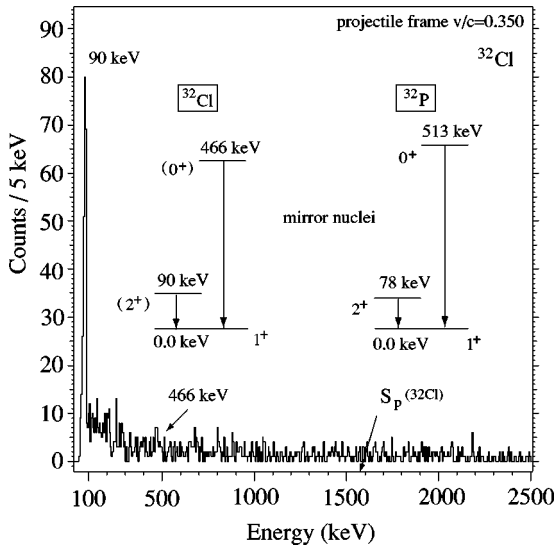

FIG. 2. γ-ray spectrum detected in the 37° ring of SeGA in coincidence with ^{32}Cl event-by-event Doppler reconstructed into the projectile frame. The 90 keV γ ray is detectable only because it is Doppler boosted well above the electronics threshold at detector angles of 37°. In the 90° ring its energy was below the detection limit. The comparison with the mirror nucleus ^{32}P is given in the inset.

The particle identification and the reconstruction of the momentum distribution of the knockout residues were performed with the focal-plane detector system of the high-resolution S800 spectrograph [17,20]. The energy loss in the S800 ion chamber, time of flight taken between scintillators, and the position and angle information of the reaction products in the focal plane of the spectrograph were employed to unambiguously identify the reaction residues behind the ^{9}Be knockout target. The spectrograph was operated in focus mode, where the incoming radioactive beam is momentum focused onto the secondary reaction target. The difference in the time of flight measured between two scintillators before the secondary target provided the particle identification of the incoming beam. Gates applied on the incoming particles allowed for a clean separation between the knockout residues and fragmentation products of the different constituents of the beam. Details about the secondary beam are summarized in Table I.

The inclusive cross sections σ_{inc} for the one-neutron knockout to all particle-stable final states were calculated from the yield of detected fragments divided by the number of incoming projectiles relative to the number density of the

TABLE I. Average midtarget beam energy (188 mg/cm^2 ^{9}Be secondary target), typical intensity, and composition of the incoming beam.

Projectile	^{32}S	^{33}Cl	^{34}Ar
Avg. midtarget E_{beam} (MeV/nucleon)	62.8	66.4	70.0
Typical avg. intensity on target (s^{-1})	920	1900	8800
Incoming cocktail beam composition (%)	8	16	76

TABLE II. One-neutron removal cross sections for the ^{9}Be(^{32}S, ^{31}S+γ)X and ^{9}Be(^{34}Ar, ^{33}Ar+γ)X reactions. Excitation energy E_x, spin and parity assignment J^π, transition energy E_γ, branching ratio BR, and resulting cross section σ compared to the calculated single-particle cross sections σ_{sp} (decomposed into a stripping σ_{sp}^{str} and diffractive part σ_{sp}^{diff}), deduced experimental and predicted (shell-model) spectroscopic factors C^2S, as well as individual theoretical cross sections σ^{th} calculated following Eq. (6) are given. For ^{33}Ar the shell model (SM) predicts two $5/2^+$ states around 3.8 MeV with sizable spectroscopic factors and therefore it is unclear to which state the proton-unbound level in ^{33}Ar compares. The inclusive cross section, the branch to the ground state from the analysis of the momentum distributions, and the reduction factor R_s are given as well (see text for more details).

	E_x (keV)	J^π ($\hbar$)	E_γ (keV)	BR (%)	σ (mb)	σ_{sp} (mb)	σ_{sp}^{str} (mb)	σ_{sp}^{diff} (mb)	C^2S Expt.	C^2S Theor.	σ^{th} (mb)
^{31}S	0.0	$1/2^+$	0.0	32.8(83)	$\leqslant$12(3)	14.1	10.7	3.4	$\leqslant$0.85(21)	0.96	14.42
	1249	$3/2^+$	1249	32.7(51)	$\leqslant$12(2)	9.8	7.7	2.1	$\leqslant$1.22(20)	0.86	8.98
	2242	$5/2^+$	2242	34.5(64)	$\leqslant$12(3)	9.4	7.4	2.0	$\leqslant$1.28(32)	1.99	19.93
	SM prediction for other (particle-bound) excited states: $\Sigma C^2S(d_{5/2})=2.28$										20.66
	$\sigma_{inc}=36(4)$ mb										
	From momentum distribution: $\sim$30(8)% [11(3) mb] to $1/2^+$ ground state										
	$R_s(^{31}\mathrm{S})=\sigma_{inc}/\sigma_{inc}^{th}=0.56(7)$										
^{33}Ar	0.0	$1/2^+$	0.0	30.2(46)	4.7(9)	12.3	9.5	2.9	0.38(7)	1.27	16.58
	1358	$3/2^+$	1358	20.2(44)	3.2(8)	8.8	7.0	1.8	0.36(9)	0.53	4.95
	1795	$5/2^+$	1795	31.7(31)	4.9(7)	8.7	6.9	1.8	0.56(8)	1.09	10.07
	3818[a]	$5/2^+$	2460	17.9(30)	2.8(6)	8.2	6.5	1.6	$\geqslant$0.34(7)		
	$\sigma_{inc}=15.6(18)$ mb										
	From momentum distribution: $\sim$27(7)% [4.2(11) mb] to $1/2^+$ ground state										
	$R_s(^{33}\mathrm{Ar})=\sigma_{inc}/\sigma_{inc}^{th}=0.41(7)$[b]										

[a]Proton unbound.

[b]Without the particle-unbound $5/2^+$ state at 3.8 MeV.

secondary ^{9}Be target (Tables II and III). The main uncertainties stem from the choice of the software gates used for particle identification (10%), the stability and purity of the beam (5%), and the correction for the momentum acceptance of the S800 spectrograph (2.5%). These systematic errors are assumed to be independent and have been added in quadrature.

From the γ-ray branching ratios and the decay level schemes (see Sec. IV for details) the cross sections for the one-neutron knockout to specific final states can be deduced from an input-output balance, and the results are summarized in Tables II and III. The intensity balance is uncertain in cases where substantial unobserved (or unassigned) γ rays are possible, and for these cases only upper limits are cited. For the γ-ray efficiency, 5% uncertainty is considered. Although an anisotropic angular distribution is expected due to alignment effects in the knockout reaction, we assume that this can be neglected in the evaluation of the intensities. The smallness of this correction is tied to the beam energy and to the particular choice of laboratory angles for the γ-ray detectors (37° and 90°) in this experiment; see the very similar example worked out in Fig. 12 of Ref. [3]. For the 90 keV γ ray observed in ^{32}Cl an uncertainty of 20% is assumed since its Doppler-shifted energy was below the lowest efficiency calibration point. The observation of the 90 keV γ ray was only possible in the 37° ring because the energy in the 90° ring was below the detection threshold.

The two position-sensitive cathode readout drift counters of the S800 focal-plane detector system in conjunction with the optics code COSY [21] served to reconstruct the longitudinal momentum of the knockout residues on an event-by-event basis. The longitudinal inclusive momentum distribution contains all knockout residues and is therefore a superposition of ground-state and excited-state contributions. The inclusive momentum distribution for ^{33}Ar is displayed in Fig. 3(a). The data points were corrected by the simulated acceptance of the spectrograph. Points where this correction exceeds a factor of 1.5 are not included. The magnetic spectrograph was operated in an optics mode where the beam is momentum focused at the position of the secondary reaction target. As a result, the momentum distribution in the S800 focal plane is broader than in the normally used "dispersion matched" mode. The momentum profile of the ^{34}Ar projectiles is shown in Fig. 3(b). Its shape is well described by a superposition of error functions.

The momentum distributions to excited levels could be determined from the coincidences with photopeaks after the correction for the underlying continuous distribution. The ground state which does not carry a separate identification must then be reconstructed by subtracting the excited-state

TABLE III. Same as Table II for the one-neutron knockout from the ^{9}Be(^{33}Cl, ^{32}Cl+γ)X reaction. Excited states labeled by (SM) are predicted by the shell model but are not observed (n.o.) in the present experiment. The USD single-particle configuration with the corresponding spectroscopic factor is listed (see text for details).

	E_x (keV)	J^π ($\hbar$)	BR (%)	σ (mb)	Conf. SM	σ_{sp} (mb)	C^2S SM	σ^{th} (mb)
^{32}Cl	0.0	1^+	62.8(85)	$\leqslant$8.2(15)	$s_{1/2}$	13.3	0.43	6.08
					$d_{3/2}$	9.8	0.05	0.52
	90	2^+	37.2(84)	$\leqslant$4.8(12)	$s_{1/2}$	13.2	0.69	9.69
					$d_{3/2}$	9.8	0.01	0.10
					$d_{5/2}$	9.8	0.04	0.42
	466	0^+	$<$10	$<$1.3	$d_{3/2}$	9.6	0.05	0.51
(SM)	1047	1^+	n.o.	n.o.	$s_{1/2}$	12.6	0.02	0.27
					$d_{5/2}$	9.4	0.03	0.30
(SM)	1135	2^+	n.o.	n.o.	$d_{3/2}$	9.4	0.22	2.20
					$d_{5/2}$	9.4	0.02	0.20
(SM)	1527	3^+	n.o.	n.o.	$d_{3/2}$	9.2	0.12	1.17
					$d_{5/2}$	9.2	0.35	3.42
From momentum distribution: $\sim$67(17)% [9(2) mb] to 1^+ ground state								
σ_{inc}=13.1(16) mb								
$R_s(^{32}\mathrm{Cl})=\sigma_{inc}/\sigma_{inc}^{th}$=0.53(7)								

distribution, properly scaled, from the inclusive momentum spectrum.

There is, however, an alternative approach applicable when the shape of the ground-state momentum distribution differs qualitatively from that for the excited states. This technique has been exploited in previous work [8,9] where noncoincident events belonged to a narrow l=0 distribution. In this case a linear combination of the momentum distributions observed in coincidence and anticoincidence with γ rays can be chosen that yields a clean narrow ground-state distribution while the coincidence events give a broader shape.

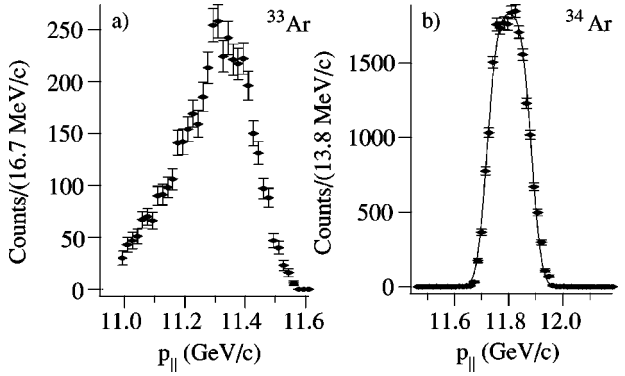

FIG. 3. Inclusive longitudinal momentum distributions of ^{33}Ar knockout residues (a) and the ^{34}Ar "unreacted" beam (b). In focus mode the beam is dispersed in the focal plane. The shape of the ^{34}Ar momentum distribution is nicely reproduced by a superposition of error functions. The theoretical momentum distributions were then folded with this curve to take into account the broadening induced by the S800 optics setting.

For ^{33}Ar, for example, the ground-state branching corresponding to this division of the data was $\approx$27(7)%, in good agreement with the direct γ-ray analysis which gave 30(5)%. This approach is independent of the analysis of the photopeaks in the γ spectra and proves consistency underlining the robustness of the analysis. For ^{32}Cl and ^{31}S this method yielded the same level of agreement (Tables II and III). The momentum distributions decomposed into ground-state and excited-state contribution are given in Figs. 4–6 and will be discussed in detail in Sec. IV.

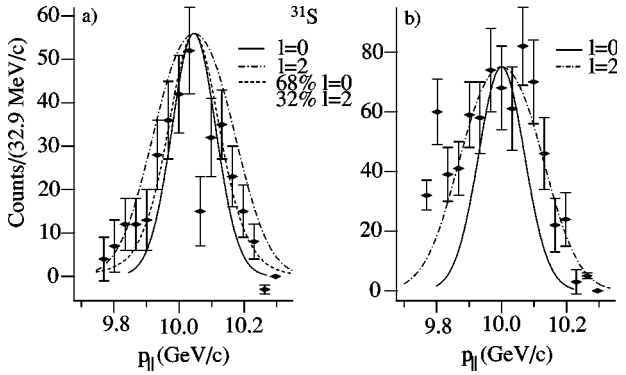

FIG. 4. Momentum distribution of ^{31}S decomposed into knockout to the ground state (a) and one-neutron removal leading to excited states (b) in the knockout residue. The excited-state distribution nicely fits with the assumption of l=2 (dashed-dotted line), while the distribution for the knockout to the ground state is best described by 68% l=0 and 32% l=2 suggesting unobserved feeding from higher-lying $5/2^+$ fragments into the ground-state distribution which is expected to be of pure l=0 character corresponding to the knockout of a neutron out of the $s_{1/2}$ orbit.

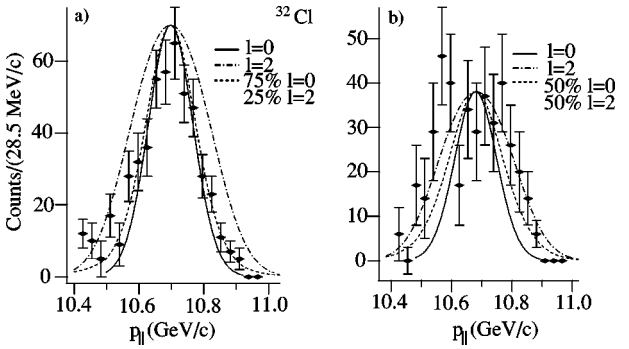

FIG. 5. Ground-state (a) and excited-state (b) momentum distributions for the one-neutron knockout residues ^{32}Cl. The shapes are compared to pure $l=2$ (dashed-dotted line), pure $l=0$ (solid line), as well as to a superposition of both (dotted line) motivated by the estimates discussed in the text.

III. THEORETICAL DESCRIPTION

A. Single-particle cross sections and momentum distributions

The individual cross sections $\sigma(I^\pi)$ for the knockout of a single nucleon with quantum numbers (n,l,j) leaving the core in a specific final state I^π can be decomposed into a part that describes nuclear structure (the spectroscopic factor C^2S) and into the contribution characterizing the reaction process (the single-particle reaction cross section σ_{sp})

$$\sigma(I^\pi) = \sum_j C^2S(j,I^\pi)\sigma_{sp}(j,S_n + E_x(I^\pi)), \tag{1}$$

with summation over all the allowed angular-momentum transfers j.

The sum $S_n + E_x(I^\pi)$ is the effective binding energy of the removed neutron where S_n is the neutron-separation energy from the ground state of the projectile and $E_x(I^\pi)$ denotes the

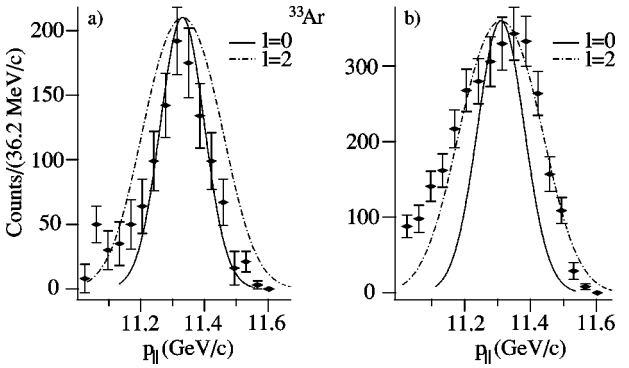

FIG. 6. Ground-state (a) and excited-state momentum distributions (b) for ^{33}Ar compared to calculations assuming $l=0$ (solid line) and $l=2$ (dashed-dotted), respectively. The narrow distribution for the knockout to the ^{33}Ar ground state is in good agreement with the calculated momentum distribution for $l=0$ knockout consistent with the expected $s_{1/2}$ configuration for the ground state of ^{33}Ar. The wider excited-state momentum distribution is nicely reproduced by $l=2$ proving that predominantly excited states with $d_{3/2}$ and $d_{5/2}$ configuration are populated in agreement with the level scheme observed.

excitation energy of the final state of the core. The single-particle cross sections are a sum of the contributions from the stripping mechanism (absorption of the neutron in the target) and diffractive dissociation (elastic breakup):

$$\sigma_{sp} = \sigma_{sp}^{str} + \sigma_{sp}^{diff} \tag{2}$$

with $\sigma_{sp}^{diff} \ll \sigma_{sp}^{str}$ for well-bound nuclei. The single-particle cross sections entering Eq. (1) were calculated within the eikonal approach of Tostevin [22]. The stripping and diffractive contributions have been computed independently from the target-core and target-neutron S matrices which were determined via Glauber theory assuming Gaussian matter distributions for core and target. The relative core-neutron wave functions were calculated in a Woods-Saxon potential. For deeply bound systems, the reaction cross section is rather sensitive to the choice of the Woods-Saxon parameters. We fixed the diffuseness consistent with previous publications [3] to $a=0.7$ fm while the radius r_0 was selected for each nucleus individually to reproduce the rms separation of neutron and core in the $1s_{1/2}$ ground state

$$r_{1s_{1/2}} = \left(\frac{A}{A-1}\right)^{1/2} r_{1s_{1/2}}^{HF} \tag{3}$$

obtained from a self-consistent Hartree-Fock (HF) approach employing the SKX Skyrme interaction [23,24]. The A-dependent coefficient takes into account that the HF radius is referred to in the nuclear center of mass. The depth of the potential was chosen to reproduce the effective binding energy of the initial state. For the core the HF matter rms radii $r_c(^{31}\mathrm{S}) = 3.10$ fm, $r_c(^{32}\mathrm{Cl}) = 3.14$ fm, and $r_c(^{33}\mathrm{Ar}) = 3.18$ fm were used. The rms radius of 2.36 fm for the ^{9}Be nuclei of the target was taken from electron scattering data [25] corrected for the point charge.

The dependence of the single-particle cross section σ_{sp} from the relative core-neutron radius $r \equiv r_{1s_{1/2}}$ and the diffuseness a can be estimated in a finite-difference approximation. For the knockout from ^{34}Ar this yields the following after evaluating the partial derivatives with respect to r and a:

$$\delta\sigma_{sp}/\sigma_{sp} = 1.286\,\delta r + 0.181\,\delta a, \tag{4}$$

where the numerical constants are in fm^{-1}. A 0.1 fm uncertainty in the radius of the single-particle orbit translates into about 13% relative error, while the cross section is rather insensitive to the parameter a. The sensitivity of σ_{sp} with respect to the core rms radius r_c can be evaluated similarly:

$$\delta\sigma_{sp}/\sigma_{sp} = -1.10\,\delta r_c. \tag{5}$$

For the one-neutron removal from ^{34}Ar to ^{33}Ar this implies a change of 0.1 fm in the core radius to result in an 11% effect which is in contrast to the case of loosely bound systems, where the sensitivity with respect to the Woods-Saxon parameters and the core radius is reduced [3]. The charge radii calculated in the SKX Hartree-Fock approach agree within 0.02 fm with the existing experimental data. Therefore, the uncertainties in the core radius and the ra-

TABLE IV. Spectroscopic factors for the ground state and the two lowest-lying excited states in ^{31}S and ^{33}P (mirror nucleus of ^{33}Ar) from transfer reactions (see Ref. [42] for the full evaluation of the ^{31}S/^{31}P data and Refs. [41,43–45] for ^{33}P).

	$C^2S(1/2_1^+)$	$C^2S(3/2_1^+)$	$C^2S(5/2_1^+)$	Reaction
^{31}S/^{31}P	1.0(1)	0.75(10)	2.1(2)	[42][a]
^{33}P	1.28	0.68	1.35	$(d,{}^3\mathrm{He})$

[a]Average of the results for the mirror pair (^{31}S/^{31}P).

dius of the single-particle orbit are expected to be of the same order of magnitude.

The shape of the momentum distribution parallel to the beam direction (longitudinal) depends on the l value of the removed neutron. The theoretical momentum distributions are calculated in the framework of a black-disk model [3,26] with the interaction radius chosen to reproduce the reaction cross sections of the free constituents. The comparison of the measured momentum distribution with theory can provide the l values involved. For the deeply bound states studied in this work the l signatures are less distinct than those for halo states and for states bound by only a few MeV. This is a phenomenon that is also encountered for angular distributions in transfer reactions; however, as the examples in the following will show, the difference between $l=0$ and $l=2$ is still big enough to provide a clear l assignment in most cases.

It is interesting that all the parallel-momentum distributions measured in the present work are asymmetric with a high-energy side that is well accounted for by the theory and with a broader distribution (a "tail") extending toward lower energies. Very similar distributions have been found in recent studies of ^{34}Si [10] and ^{57}Ni [27]. These asymmetric shapes can only be explained by effects that go beyond eikonal theory. We have observed an apparently similar, but probably fundamentally different, phenomenon in the $l=0$ cross sections of the halo nuclei ^{11}Be and ^{15}C [28]. There it could be traced to the elastic breakup mechanism and accounted for by a theory that included couplings to the continuum, very important for halo systems, and that allowed for an exact treatment of the three-body reaction dynamics. This explanation does not apply to the present cases, which are deeply bound and for which diffraction dissociation is a minor part of the cross section. Understanding the asymmetric shapes remains an interesting challenge, but the problem is, in all likelihood, not essential to our applications of knockout reactions for spectroscopic purposes. We suspect that, similar to the ^{11}Be and ^{15}C cases, the integrated partial cross section will be accounted for by the eikonal theory, so that the effect amounts to a redistribution of the differential cross section.

As outlined before, the spectrograph was operated in focused mode resulting in a broadened momentum distribution, which was accounted for by convoluting the theoretical momentum profiles with the momentum distribution of the "unreacted" projectile beam passing through the ^{9}Be target [Fig. 3(b)].

B. Shell-model predictions

Spectroscopic factors for ^{31}S, ^{32}Cl, and ^{33}Ar were calculated in the *sd* shell model using the USD effective interaction [29]. The configurations are $\pi(sd)^8\nu(sd)^7$, $\pi(sd)^9\nu(sd)^7$, and $\pi(sd)^{10}\nu(sd)^7$, respectively. The WBT *sd* Hamiltonian [30] was used and all calculations were performed with the code OXBASH [31].

The inclusive cross section predicted by theory can then be written as

$$\sigma_{inc}^{th} = \sum_{E_x(I^\pi)\leqslant S_p} \sum_j \left(\frac{A}{A-1}\right)^2 C^2S(I^\pi,j)\,\sigma_{sp}(j,S_n+E_x(I^\pi)) \tag{6}$$

$$= \sum_{E_x(I^\pi)\leqslant S_p} \sigma^{th}(I^\pi), \tag{7}$$

where the σ_{sp} are the single-particle cross sections calculated in the eikonal model explained in the preceding section, and C^2S are the spectroscopic factors from shell model. The A-dependent term is a center-of-mass correction [32,33] for the *sd* shell. The sum extends over all particle-bound states and possible angular-momentum transfers j. The shell-model predictions are summarized in Tables II and III and discussed in the following section.

IV. DISCUSSION

The experimental results, calculated single-particle cross sections, and shell-model predictions (configurations as well as spectroscopic factors) are summarized in Table II for ^{31}S and ^{33}Ar and in Table III for the knockout to the odd-odd nucleus ^{32}Cl. Experimental spectroscopic factors are given as the ratio of the experimental cross section and the single-particle cross section calculated according to the reaction theory outlined before. In the following, the three knockout reactions and the reduction in spectroscopic strengths with respect to the USD shell model are discussed in detail.

The neutron single-particle structure of ^{31}S has been studied extensively with (p,d) [34,35], (d,t) [36–38], and $(^3\mathrm{He},\alpha)$ [39,40] transfer reactions at low energies (see Refs. [41,42] for the evaluated summaries). Nothing was known previously for the neutron single-particle structure in ^{32}Cl from transfer reactions, while for ^{33}Ar the spectroscopic information can be compared to the results of ^{34}S$(d,{}^3\mathrm{He})^{33}$P transfer [43–45] sensing the corresponding proton hole states in the mirror ^{33}P. The prior results on ^{31}S and ^{33}P are summarized in Table IV.

A. ^{9}Be(^{32}S, ^{31}S + γ)X

A variety of population mechanisms have been employed to establish the level scheme of ^{31}S [41]. In the present one-neutron knockout measurement of ^{32}S the first two excited states of ^{31}S are observed [the first $3/2^+$ level at 1249(7)keV and the first $5/2^+$ state at 2242(9) keV]. The lower panel of Fig. 1 displays the γ-ray spectrum event-by-event Doppler reconstructed into the projectile frame, detected in coincidence with knockout residues.

From the three one-neutron knockout residues reported in this paper, ^{31}S has the highest proton-separation energy with $S_p=6133.3(16)$ keV. From the shell-model calculation

higher-lying $5/2^+$ states below the proton-separation energy are expected to be populated. Due to low statistics and the decreasing efficiency of germanium detectors with increasing γ-ray energy, the transitions depopulating these higher-lying levels are easily below the sensitivity limit of the experiment. According to the shell-model calculation a sizable fraction of the $d_{5/2}$ spectroscopic strength, $\Sigma C^2S(d_{5/2})=2.28$, is fragmented over several $5/2^+$ states between 3 MeV and the proton-separation energy $S_p=6.13$ MeV. Indirect feeding is a challenge in knockout experiments on deeply bound systems and it has to be determined from an input-output balance. In this experiment it is not possible to disentangle the amount of direct population of the observed states in knockout from the indirect feeding by unobserved higher-lying states. The spectroscopic factors deduced from the experiment are therefore upper limits.

Due to the indirect feeding, the momentum distribution attributed to ^{31}S knockout residues in the ground state is very likely to be contaminated by an $l=2$ contribution [Fig. 4(a)]. The calculated momentum distribution assuming pure $l=0$ (solid line) from the knockout of a $s_{1/2}$ neutron underestimates the width of the momentum distribution observed in the experiment. However, a decomposition into $0.68f_{p_\parallel}(l=0)+0.32f_{p_\parallel}(l=2)$ nicely reproduces the data (dotted line). The shape of the parallel-momentum distribution of ^{31}S in coincidence with excited states [Fig. 4(b)] is in agreement with the assumption of $l=2$ angular-momentum transfer (dashed line) corresponding to the expected removal of one neutron from the $0d_{3/2}$ and $0d_{5/2}$ orbitals.

Following the strategy outlined above, the single-particle cross sections σ_{sp} for the one-neutron removal were derived with Woods-Saxon parameters of $a=0.7$ fm and $r_0=1.25$ fm to match the rms neutron-core separation of the SKX Hartree-Fock $1s_{1/2}$ ground state, predicted to be $r=3.46$ fm. The experimental results and calculations are summarized in Table II.

B. ^{9}Be(^{33}Cl, ^{32}Cl+γ)X

The level scheme of ^{32}Cl is known from the β decay of ^{32}Ar [41]. In coincidence with ^{32}Cl residues we clearly observe the 90 keV transition of the first excited state and see weak hints of the 466 keV transition as well. Figure. 2 shows the γ-ray spectrum observed in the 37° ring. Due to the Doppler boost the 90 keV peak is only visible at 37°, in the 90° ring it is below the detection threshold. A comparison with the mirror nucleus and tentative spin assignments are given as inset.

In the knockout to odd-odd nuclei the final state is in general mixed and has to be decomposed into single-particle contributions. In ^{32}Cl, for example, the 1^+ ground state contains $s_{1/2}$ as well as $d_{3/2}$ components indicated by the nonzero spectroscopic factors for the corresponding configuration (Table III).

The $1_2^+, 2_2^+$, and 3_1^+ states below the proton-separation energy of $S_p=1575(7)$ keV [46] are predicted to be accessible via one-neutron removal from ^{33}Cl to ^{32}Cl. Due to low statistics the depopulating transitions of these states were not seen in the present experiment. However, this unobserved feeding becomes apparent by looking at the momentum distributions displayed in Figs. 5(a) and 5(b). The ground-state distribution extracted from the experiment is broader than pure $l=0$ angular-momentum transfer. About 9% $l=2$ is expected from the $d_{3/2}$ component in the configuration of the 2_1^+ state itself (see Table III). Further, by using the spectroscopic factors provided by the shell model and the single-particle cross sections from the reaction model in conjunction with γ-ray branching ratios taken from the $1_2^+, 2_2^+$, and 3_1^+ states in the mirror nucleus ^{32}P an indirect feeding of about 20% $l=2$ from these higher-lying bound states is likely to be included in the experimental ground-state momentum distribution presented in Fig. 5(a). The best agreement between experiment and calculated shape is reached by assuming $f_{p_\parallel}=0.75f_{p_\parallel}(l=0)+0.25f_{p_\parallel}(l=2)$ (dotted curve) which is very close to the estimates outlined above, but pure $l=0$ is not excluded.

The parallel-momentum distribution detected in coincidence with the 90 keV γ-ray transition [Fig. 5(b) is expected to be a superposition of $l=0$ and $l=2$ contributions as well. From the shell model, the configuration is dominated by $s_{1/2}$. However, unobserved feeding from the states with $d_{3/2}$ and $d_{5/2}$ components is likely to contribute. Employing shell-model spectroscopic factors C^2S, calculated reaction cross sections σ_{sp}, and decay branching ratios of the corresponding states in the mirror ^{32}P the experimental momentum distribution can be decomposed into $\approx$57% $l=0$ and 43% $l=2$. Calculations assuming pure $l=0$ (solid line), pure $l=2$ (dashed-dotted), and $f_{p_\parallel}=0.50f_{p_\parallel}(l=0)+0.50f_{p_\parallel}(l=2)$ (dashed) are compared to the measured points. The experimental data seem best described by the broad $l=2$ shape, the assumption of 50% $l=0$ contribution is still in agreement with the measurement while a pronounced dominance of $l=0$ can be excluded. However, the large error bars prevent a more definitive conclusion on the detailed composition of the momentum distribution detected in coincidence with the 2_1^+ state of ^{32}Cl.

In this case the single-particle cross sections σ_{sp} within the eikonal model used the Woods-Saxon parameters $a=0.7$ fm with the radius parameter $r_0=1.26$ fm chosen to reproduce the rms core-neutron separation of 3.46 fm of the $s_{1/2}$ orbit obtained by the Hartree-Fock calculation. Experimental results as well as theory predictions are given in Table III.

C. ^{9}Be(^{34}Ar, ^{33}Ar+γ)X

The first information on excited states of ^{33}Ar stems from mass excess measurements performed with an ^{36}Ar(^{3}He, ^{6}He) reaction in 1974 [47]. Aside from the $1/2^+$ ground state, two excited states at 1344(2) keV and 1786(20) keV were observed. By analogy with the mirror nucleus ^{33}P, spin and parity assignments of $3/2^+$ and $5/2^+$ were proposed [47], respectively. Recently, in a ^{34}Ar secondary fragmentation experiment on a polypropylene target, the level scheme was confirmed with significantly reduced uncertainty in the energies and was extended to higher excitation energies [48].

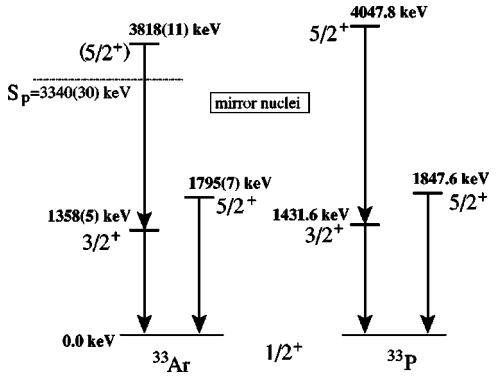

FIG. 7. Excited states observed in ^{33}Ar compared to the mirror nucleus ^{33}P. The second $5/2^+$ state is proton unbound. This level scheme is in agreement with a recent in-beam fragmentation experiment [48].

In the present experiment the depopulating γ-ray transitions of the first $3/2^+$ excitation, the first $5/2^+$ state, and a higher-lying $5/2^+$ level could be observed. The $5/2^+$ spin assignment comes from theory and a comparison with the mirror nucleus; our technique is not able to distinguish $d_{3/2}$ and $d_{5/2}$. All assignments (and cross sections) are consistent with the shell model. The γ-ray spectrum detected in coincidence with the ^{33}Ar knockout residues is given in the upper panel of Fig. 1. A comparison with the mirror ^{33}P suggests in agreement with shell-model calculations that the 2460 keV γ ray depopulates the proton unbound $5/2^+$ level at 3818(11) keV. In Fig. 7 the comparison to the mirror nucleus is given and reinforces the spin assignments for ^{33}Ar.

The proton-separation energy of ^{33}Ar is with $S_p = 3340(30)$ keV [46] low compared to ^{31}S and ^{32}Cl. Unlike the cases discussed above unobserved feeding from higher-lying states is not expected. In fact, we observed the transitions of all states below the proton-separation energy which, according to the shell-model calculation, are populated in one-neutron knockout. This is also reflected in the momentum distributions for the knockout to the ground state and to all excited states shown in Figs. 6(a) and 6(b), the narrow momentum distribution for ^{33}Ar nuclei in the ground state is in excellent agreement with the assumption of pure $l=0$ angular momentum while the distribution in coincidence with all excited states is well reproduced by $l=2$, corresponding to the expected knockout of a neutron out of $0d_{3/2}$ and $0d_{5/2}$ orbits.

The single-particle cross sections were calculated with the diffuseness of the Woods-Saxon potential fixed to $a = 0.7$ fm and with the radius $r_0 = 1.28$ fm to reproduce the corresponding rms core-neutron separation of $r = 3.45$ fm for the ground-state $1s_{1/2}$ orbital calculated in the Skyrme SKX Hartree-Fock approach. The results of the analysis are summarized in Table II.

D. Quenching

Following the method discussed in Ref. [7] we define the reduction factor R_s as the ratio of the experimental and theoretical inclusive cross sections:

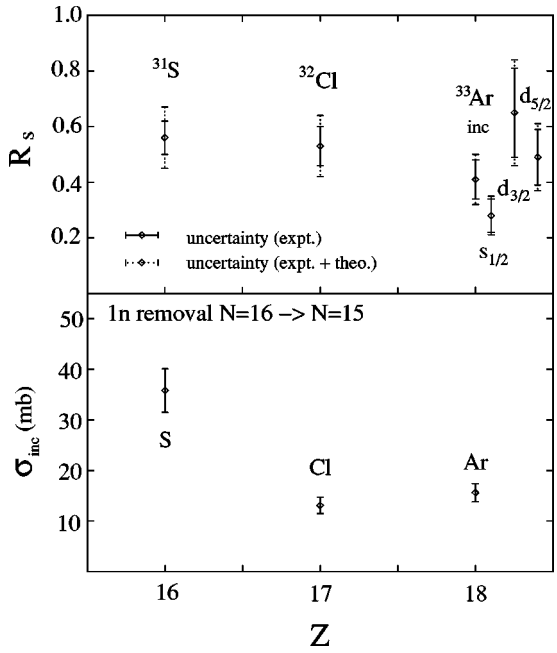

FIG. 8. Reduction factors R_s and inclusive cross sections for the one-neutron removal reactions ^{9}Be(^{32}S, ^{31}S+γ)X, ^{9}Be(^{33}Cl, ^{32}Cl+γ)X, and ^{9}Be(^{34}Ar, ^{33}Ar+γ)X. Two sets of error bars are given for R_s, solely the experimental uncertainty (solid line style) and error bars with a 15% uncertainty added in quadrature attributed to the reaction theory and its sensitivity to the Woods-Saxon potential and the core radius (dotted line style).

$$R_s = \frac{\sigma_{inc}^{exp}}{\sigma_{inc}^{th}}. \tag{8}$$

For all three one-neutron knockout reactions discussed in the present paper a reduction factor R_s of about 0.5 has been observed. For the case of ^{33}Ar we exclude the particle-unbound $5/2^+$ state at 3.8 MeV from the calculation of R_s, since this state possibly decays in part by (unobserved) proton emission. This is consistent with the results from $(e,e'p)$ [13] and $(d,{}^3\mathrm{He})$ [14] reactions on stable, well bound, and near-magic systems and is in agreement with quenching found following the one-neutron and one-proton knockout on deeply bound (binding energies >10 MeV) light carbon and oxygen nuclei [3,7] performed with different targets and at various beam energies. This reduction in the single-particle occupancy is attributed to the incomplete treatment of the strongly repulsive core and the tensor part of the nucleon-nucleon interaction in the conventional shell model based on effective interactions [13].

The absolute spectroscopic factors deduced from the transfer reactions quoted in Table IV are in agreement with the USD shell model. However, as demonstrated for several cases in Ref. [14] various uncertainties in the early analyses of transfer reaction cross sections can change the absolute spectroscopic factors and finally result in a reduction of 50–60% consistent with the findings of the present experiment.

In the regime of high neutron binding energy and accounting for the reaction theory's sensitivity to the Woods-Saxon potential and to the core rms radius, a maximum uncertainty of 15% has been added in quadrature to the experimental errors quoted in Tables II and III. These error bars are shown in addition to the solely experimental uncertainties in the upper panel of Fig. 8.

The indirect feeding from higher-lying states apparent in the knockout to ^{31}S and ^{32}Cl prevents an analysis of the reduction R_s for individual single-particle orbits. However, in ^{33}Ar all states below the proton-separation energy S_p predicted to be populated in one-neutron removal have been observed in the experiment, and individual reduction factors for the $s_{1/2}, d_{3/2}$, and $d_{5/2}$ orbits can be evaluated separately (Fig. 8). In this case the reduction factor R_s equals the ratio of the experimental and shell-model spectroscopic factor. Especially remarkable is the low R_s found for the $1/2^+$ state in the knockout from ^{34}Ar, with its separation energy of 17 MeV the most deeply bound state studied so far. The results indicate that the amount of quenching might be different for different single-particle configurations involved but a more definitive conclusion certainly needs reduced error bars and more cases to be studied.

V. SUMMARY

The proton-rich $N=15$ isotones with $Z=16,17$, and 18 have been investigated at the Coupled Cyclotron Facility of the NSCL using the one-neutron knockout reactions ^{9}Be(^{32}S, ^{31}S$+\gamma$)X, ^{9}Be(^{33}Cl, ^{32}Cl$+\gamma$)X, and ^{9}Be(^{34}Ar, ^{33}Ar $+\gamma$)X in inverse kinematics. Employing γ-ray spectroscopy with SeGA and particle detection with the high-resolution S800 spectrograph has allowed inclusive cross sections and cross sections for the population of individual excited states to be measured.

The momentum distributions of the knockout residues were used to extract information on the angular momentum l of the knockedout neutron. Further, the use of intermediate beam energies allowed a theoretical description of the reaction process within an eikonal approach in sudden approximation. The dependency of the theoretical single-particle cross sections from the Woods-Saxon parameters and the rms radius of the core is discussed and, in contrast to loosely bound systems, found to be significant. Consequently, the choice of parameters has been justified in comparison to the core-neutron relative radius of the $1/2^+$ ground state predicted within a self-consistent Hartree-Fock approach employing the SKX Skyrme interaction.

A reduction of the experimental spectroscopic strength with respect to a USD shell-model calculation has been observed and extends the systematics established so far for stable and near-magic systems from $(e,e'p)$ and $(d,{}^3\mathrm{He})$ reactions and for deeply bound light nuclei around carbon and oxygen from one-nucleon knockout experiments.

ACKNOWLEDGMENTS

We thank A. Stolz, T. Ginter, M. Steiner, and the NSCL cyclotron operations group for providing the high-quality secondary and primary beams. The authors acknowledge discussions with A.F. Lisetskiy, J.-L. LeCouey, K. Yoneda, O. Tarasov, and R.R.C. Clement. This work was supported by the National Science Foundation under Grants No. PHY-0110253, PHY-9875122, PHY-0244453, and PHY-0342281.

[1] J. A. Tostevin, J. Phys. G **25**, 735 (1999).
[2] P. G. Hansen and B. M. Sherrill, Nucl. Phys. **A693**, 133 (2001).
[3] P. G. Hansen and J. A. Tostevin, Annu. Rev. Nucl. Part. Sci. **53**, 219 (2003).
[4] T. Aumann, A. Navin, D. P. Balamuth, D. Bazin, B. Blank, B. A. Brown, J. E. Bush, J. A. Caggiano, B. Davids,T. Glasmacher, V. Guimarães, P. G. Hansen, R. W. Ibbotson, D. Karnes, J. J. Kolata, V. Maddalena, B. Pritychenko, H. Scheit, B. M. Sherrill, and J. A. Tostevin, Phys. Rev. Lett. **84**, 35 (2000).
[5] V. Guimarães, J. J. Kolata, D. Bazin, B. Blank, B. A. Brown, T. Glasmacher, P. G. Hansen, R. W. Ibbotson, D. Karnes, V. Maddalena, A. Navin, B. Pritychenko, B. M. Sherrill, D. P. Balamuth, andJ. E. Bush, Phys. Rev. C **61**, 064609 (2000).
[6] A. Navin, D. W. Anthony, T. Aumann, T. Baumann, D. Bazin, Y. Blumenfeld, B. A. Brown, T. Glasmacher, P. G. Hansen, R. W. Ibbotson, P. A. Lofy, V. Maddalena, K. Miller, T. Nakamura, B. V. Pritychenko, B. M. Sherrill, E. Spears, M. Steiner, J. A. Tostevin, J. Yurkon, and A. Wagner, Phys. Rev. Lett. **85**, 266 (2000).
[7] B. A. Brown, P. G. Hansen, B. M. Sherrill, and J. A. Tostevin, Phys. Rev. C **65**, 061601(R) (2002).
[8] A. Navin, D. Bazin, B. A. Brown, B. Davids, G. Gervais, T. Glasmacher, K. Govaert, P. G. Hansen, M. Hellström, R. W. Ibbotson, V. Maddalena, B. Pritychenko, H. Scheit, B. M. Sherrill, M. Steiner, J. A. Tostevin, and J. Yurkon, Phys. Rev. Lett. **81**, 5089 (1998).
[9] V. Maddalena, T. Aumann, D. Bazin, B. A. Brown, J. A. Caggiano, B. Davids, T. Glasmacher, P. G. Hansen, R. W. Ibbotson, A. Navin, B. V. Pritychenko, H. Scheit, B. M. Sherrill, M. Steiner, J. A. Tostevin, and J. Yurkon, Phys. Rev. C **63**, 024613 (2001).
[10] J. Enders, A. Bauer, D. Bazin, A. Bonaccorso, B. A. Brown, T. Glasmacher, P. G. Hansen, V. Maddalena, K. L. Miller, A. Navin, B. M. Sherrill, and J. A. Tostevin, Phys. Rev. C **65**, 034318 (2002).
[11] G. J. Kramer, H. P. Blok, J. F. A. van Hienen, S. Brandenburg, M. N. Harakeh, Y. Y. van der Werf, P. W. M. Glaudemans, and A. A. Wolters, Nucl. Phys. **A477**, 55 (1988), and references therein.
[12] J. W. A. den Herder, H. P. Blok, E. Jans, P. H. M. Keizer, L. Lapikas, E. N. M. Quint, G. van der Steenhoven, and P. K. A. de Witt Hubers, Nucl. Phys. **A490**, 507 (1988), and references therein.
[13] V. R. Pandharipande, I. Sick, and P. K. A. de Witt Huberts, Rev. Mod. Phys. **69**, 981 (1997).

[14] G. J. Kramer, H. P. Blok, and L. Lapikas, Nucl. Phys. **A679**, 267 (2001).
[15] J. Enders, T. Baumann, B. A. Brown, N. H. Frank, P. G. Hansen, P. R. Heckman, B. M. Sherrill, A. Stolz, M. Thoennessen, J. A. Tostevin, E. J. Tryggestad, S. Typel, and M. S. Wallace, Phys. Rev. C **67**, 064301 (2003).
[16] D. J. Morrissey, B. M. Sherrill, M. Steiner, A. Stolz, and I. Wiedenhöver, Nucl. Instrum. Methods Phys. Res. B **204**, 90 (2003).
[17] D. Bazin, J. A. Caggiano, B. M. Sherrill, J. Yurkon, and A. F. Zeller, Nucl. Instrum. Methods Phys. Res. B **204**, 629 (2003).
[18] W. F. Mueller, J. A. Church, T. Glasmacher, D. Gutknecht, G. Hackman, P. G. Hansen, Z. Hu, K. L. Miller, and P. Quirin, Nucl. Instrum. Methods Phys. Res. A **466**, 492 (2001).
[19] GEANT-detector description and simulation tool, version 3.21, CERN Program Library Long Writeup W5013, 1994.
[20] J. Yurkon, D. Bazin, W. Benenson, D. J. Morrissey, B. M. Sherrill, D. Swan, and R. Swanson, Nucl. Instrum. Methods Phys. Res. A **422**, 291 (1999).
[21] M. Berz, K. Joh, J. A. Nolen, B. M. Sherrill, and A. F. Zeller, Phys. Rev. C **47**, 537 (1993).
[22] J. A. Tostevin, Nucl. Phys. **A682**, 320c (2001).
[23] B. A. Brown, Phys. Rev. C **58**, 220 (1998).
[24] B. A. Brown, W. A. Richter, and R. Lindsay, Phys. Lett. B **483**, 49 (2000).
[25] H. De Vries, C. W. De Jager, and C. De Vries, At. Data Nucl. Data Tables **36**, 495 (1987).
[26] P. G. Hansen, Phys. Rev. Lett. **77**, 1016 (1996).
[27] K. L. Yurkewicz *et al.* (unpublished).
[28] J. A. Tostevin, D. Bazin, B. A. Brown, T. Glasmacher, P. G. Hansen, V. Maddalena, A. Navin, and B. M. Sherrill, Phys. Rev. C **66**, 024607 (2002).
[29] B. A. Brown and B. H. Wildenthal, Annu. Rev. Nucl. Part. Sci. **38**, 29 (1988); B. H. Wildenthal, Prog. Part. Nucl. Phys. **11**, 5 (1984).
[30] E. K. Warburton and B. A. Brown, Phys. Rev. C **46**, 923 (1992).
[31] B. A. Brown, A. Etchegoyen, W. D. M. Rae, N. S. Godwin, W. A. Richter, C. H. Zimmermann, W. E. Ormand, and J. S. Winfield, MSU-NSCL Report No. 524, 1985 (unpublished).
[32] A. E. L. Dieperink and T. de Forest, Phys. Rev. C **10**, 543 (1974).
[33] B. A. Brown, A. Csoto, and R. Sherr, Nucl. Phys. **A597**, 66 (1996).
[34] R. L. Kozub, Phys. Rev. **172**, 1078 (1968).
[35] B. M. Mayer, J. Gosset, J. L. Escudie, and H. Kamitsubo, Nucl. Phys. **A177**, 205 (1971).
[36] C. A. Whitten, Jr., M. C. Mermaz, and D. A. Bromley, Phys. Rev. C **1**, 455 (1970).
[37] T. G. Dzubay and R. V. Poore, Phys. Rev. C **5**, 1304 (1972).
[38] R. E. Tribble and K. I. Kubo, Nucl. Phys. **A282**, 269 (1977).
[39] T. S. Bhatia and W. W. Daehnick, Phys. Rev. C **5**, 111 (1971).
[40] C. E. Moss, Nucl. Phys. **A145**, 423 (1970).
[41] P. M. Endt, Nucl. Phys. **A633**, 1 (1998).
[42] P. M. Endt, At. Data Nucl. Data Tables **19**, 23 (1977).
[43] R. C. Bearse, D. H. Youngblood, and J. L. Yntema, Phys. Rev. **167**, 1048 (1968).
[44] C. E. Thorn, J. W. Olness, E. K. Warburton, and S. Raman, Phys. Rev. C **30**, 1442 (1984).
[45] S. Khan, G. Mairle, K. T. Knopfle, Th. Kim, L.-K. Pao, P. Grabmayr, G. J. Wagner, and L. Friedrich, Nucl. Phys. **A253**, 253 (1988).
[46] G. Audi and A. H. Wapstra, Nucl. Phys. **A595**, 409 (1995).
[47] H. Nann, W. Benenson, E. Kashy, and P. Turek, Phys. Rev. C **9**, 1848 (1974).
[48] R. R. C. Clement, Ph.D. thesis, Michigan State University, 2003.